Static stress analysis of coupling superconducting solenoid coil assembly for muon ionization cooling experiment

PAN Heng* WANG Li WU Hong GUO Xinglong XU Fengyu

Institute of Cryogenics and Superconductivity Technology, Harbin Institute of Technology, Harbin 150080, China

Abstract The stresses in the coupling superconducting solenoid coil assembly, which is applied in the Muon Ionization Cooling Experiment (MICE), are critical for the structure design and mechanical stability because of a large diameter and relative high magnetic field. This paper presents an analytical stress solution for the MICE coupling coil assembly. The stress due to winding tension is calculated by assuming the coil package as a set of combined cylinders. The thermal and electromechanical stresses are obtained by solving the partial differential equations of displacement based on the power series expansion method. The analytical stress solution is proved to be feasible by calculating stresses in a tested superconducting solenoid with 2.58 m bore at room temperature. The analytical result of the MICE coupling coil is in good agreement with that of the finite element which shows that the transverse shear stress induced by Lorentz force is principally dominant to magnet instability.

Key words MICE superconducting magnet, Stress analysis, Mechanical stability

1 Introduction

The Muon Ionization Cooling Experiment (MICE) will demonstrate ionization cooling in a short section of a realistic cooling channel using a muon beam at Rutherford Appleton Laboratory, UK[1]. The coupling superconducting magnet is a key equipment in the MICE cooling channel, which can provide a magnetic field of 2.6 T at the centerline so that the beam runs in the thin windows of the radio frequency cavity[2,3]. The coupling coil wound by the conductor of 96 layers has an inner radius of 750mm, in which the peak induction is around 7.4 T at a full current of 210 A for the worst operation case of the MICE channel.

The stresses induced by the MICE coupling coil assembly are relatively high due to its large diameter and huge magnetic field. Analyzing the stress of the coupling magnet is essential for the design process. Historically, the analytical solutions have been limited to two dimensions with assumptions only suitable to the coil mid-plane, and the shear stress is assumed to be negligible[4-6]. However, the total stress components can be solved by a finite element model using a particular program in a specific magnet. Considering the shear stress based on power series method or Green's function, a few analytical calculations have been reported on the electromechanical stresses[7,8].

In this paper, we formulate and solve a three dimensional analysis of stresses induced by winding tension, thermal, and magnetic load. The properties of anisotropic materials are employed in the analysis, The initial stresses caused by winding tension are calculated under the combined cylinder assumption, and the thermally and magnetically induced stresses are solved by transforming the displacement Partial Differential Equations (PDE) to Ordinary Differential Equations (ODE) using the method of power series expansion. Compared with the reported models, the shear stress and axial stress beyond the mid-plane of the coil can be analyzed by the present solution. It is not limited to solve the stresses due to the magnetic load, and is closer to the practical situation than the

Supported by Funds of cryogenics and superconductivity technology innovation project under "985-2 Plan" of Harbin Institute of Technology, China and by the Office of Science, US Department of Energy under DOE contract DE-AC02-05CH11231

* Corresponding author. *E-mail address:* panheng@hit.edu.cn

Received date: 2009-08-28

reported results. The results indicate that the shear stress induced by thermal and magnetic load leads to the crack of epoxy resin to dissipate strain energy.

2 The MICE coupling coil assembly

The coupling coil assembly can be divided into coil package, banding, mandrel and insulations. The coil package consists of fiberglass cloth, epoxy resin, and superconductors, which is wrapped by 5356 aluminum alloy wire. The mandrel fabricated by a 6061-T6 aluminum alloy includes three sections of bobbin, end plates, and cover plate (in thickness of 19, 18, and 45 mm, respectively), and the insulated G-10 plates stand between the coil and mandrel. The cooling cryogen flows in the cover plate through a nested piping to cool the coil by conduction. Fig. 1 shows the cross section of the coupling coil assembly. Z is the axial direction, and R is the radial direction.

The Lorentz force is outward in radial direction when the coil is energized, so the stress decreases in the coil bobbin, whereas it increases in the coil and banding. The stresses in the two end plates and the cover plate are smaller than that of the coil. Therefore, analytical model of the coil assembly should consist of the banding, the coil package and the bobbin.

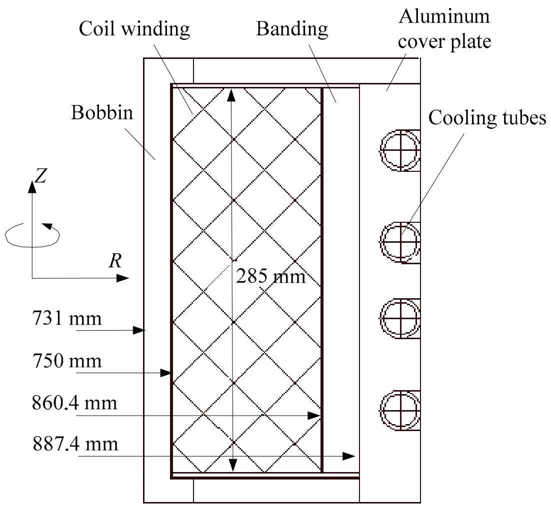

Fig. 1 The crosssection of MICE coupling coil assembly.

3 Analytical model

3.1 Stress equilibrium equations

Given the coil package behaves as an orthotropic manner, the analytical model is a linear elastic homogeneous body with transversely isotropic properties, which is used as an effective anisotropic elastic modulus by using the micro-mechanics finite element method [9]. The shear stresses in the r-θ plane and z-θ plane are zero due to inherently axisymmetric geometry, and there is no coupling between normal stress and shear stress. Here, the stress tensor has four components in the cross-section of the coil assembly. The stress equilibrium equations for the coil assembly are:

$$r\frac{\partial}{\partial r}\sigma_r + \sigma_r - \sigma_\theta + r\frac{\partial}{\partial z}\tau_{rz} + rF_r = 0 \qquad (1)$$

$$r\frac{\partial}{\partial r}\tau_{rz} + \tau_{rz} + r\frac{\partial}{\partial z}\sigma_z + rF_z = 0 \qquad (2)$$

where, F_r and F_z are the radial and axial component of Lorentz force which are functions of r and z, and are relative to the current density and magnetic field [10]:

$$\boldsymbol{F} = \boldsymbol{J}\times\boldsymbol{B} \qquad (3)$$

The stress equilibrium equations for the banding and bobbin are derived separately, in which the item of body force is zero. Considering thermal strain for an orthotropic material, the strain-stress relation is:

$$\varepsilon_i = \frac{\sigma_i}{E_i} - \sum_{\substack{j=r\\ j\neq i}}^{z}\left(\nu_{ji}\frac{\sigma_j}{E_j}\right) + \alpha_i\Delta T, \quad i = r,\ \theta,\ z$$

$$\gamma_{rz} = \frac{\tau_{rz}}{G_{rz}} \qquad (4)$$

where, α_i is the integral secant coefficient of thermal expansion. The displaced U_r and U_z at each point of the coil assembly are functions of r and z. The strain-displacement relations are:

$$\varepsilon_r = U_{r,r}, \quad \varepsilon_\theta = \frac{U_r}{r}, \quad \varepsilon_z = U_{z,z}, \quad \gamma_{rz} = U_{r,z} + U_{z,r} \qquad (5)$$

The total stresses are summed by the initial stresses, thermal contraction and magnetic load [11]:

$$\sigma = \sigma^W + \sigma^T + \sigma^{\mathrm{M}} \qquad (6)$$

where, σ^{W} is initial stresses of the winding tension, σ^{T} is thermally induced stresses, and σ^{M} is magnetically induced stresses.

3.2 Stress induced by winding tension

The items of body force in Eqs.(1) and (2) are zero if there is no magnetic load on the coil. The axial stress and shear stress are negligible if there is no axial load on the conductor. When the temperature difference in Eq.(3) is zero, the stress equilibrium is:

$$r\frac{\partial}{\partial r}\sigma_r+\sigma_r-\sigma_\theta=0 \tag{7}$$

Each conducted layer is regarded as a thinwall cylinder to which the winding tension is applied and is subsequently assembled into the coil by the stresses harmony among layers. According to the combined cylinder theory, the hoop stress in the k^{th} layer after winding is:

$$\sigma_\theta^{\mathrm{W}}=\sum_{i=k}^{96}\left[\frac{-P_{i+1}R_i^2}{R_i^2-r_{\mathrm{i\_bobbin}}^2}\left(1+\frac{r_{\mathrm{i\_bobbin}}^2}{\left(R_i-\frac{1}{2}\delta\right)^2}\right)\right]+\sigma_{\mathrm{pre}} \tag{8}$$

and the radial pressure to the bobbin is:

$$\sigma_r^{\mathrm{W}}=\sum_{i=0}^{95}\left[\frac{-P_{i+1}R_i^2}{R_i^2-r_{\mathrm{i\_bobbin}}^2}\left(1+\frac{r_{\mathrm{i\_bobbin}}^2}{r_{\mathrm{o\_bobbin}}^2}\right)\right] \tag{9}$$

where, R_i is an outer radius of layer (i),
$r_{\mathrm{i\_bobbin}}$ is an inner radius of bobbin,
$r_{\mathrm{o\_bobbin}}$ is an outer radius of bobbin,
P_{i+1} is a pressure between i+1 and i,
σ_{pre} is a constant prestress of conductor,
δ is a thickness of layer.

3.3 Stress induced by thermal contraction

In the case of thermal stress, the body force is zero, and the temperature difference in Eq.(3) is 296 K. If the constant axial strain is assumed to simplify calculation, by substituting Eqs.(1) and (2) with Eq.(4) the stress equilibrium equations can be

$$r^2\frac{\partial^2 U_r}{\partial r^2}+a_1r^2\left(\frac{\partial^2 U_z}{\partial r\partial z}\right)+a_2r^2\frac{\partial^2 U_r}{\partial z^2}+r\frac{\partial U_r}{\partial r}+a_3U_r+a_4r\varepsilon_z=0 \tag{10}$$

$$r\frac{\partial^2 U_z}{\partial r^2}+r\frac{\partial^2 U_r}{\partial r\partial z}+\frac{\partial U_r}{\partial z}+\frac{\partial U_z}{\partial r}=0 \tag{11}$$

where, a_1 to a_4 are the stiffness coefficients. This analysis expresses the displacement U_r and U_z as a power series forms with respect to z [8]:

$$\sigma_{\mathrm{r0}}^{\mathrm{bobbin}}=0,\sigma_{\mathrm{r1}}^{\mathrm{coil}}=\sigma_{\mathrm{r1}}^{\mathrm{bobbin}},\ \sigma_{\mathrm{r2}}^{\mathrm{coil}}=\sigma_{\mathrm{r2}}^{\mathrm{banding}},\sigma_{\mathrm{r3}}^{\mathrm{banding}}=p_{\mathrm{cover}}$$

$$U_{\mathrm{r2}}^{\mathrm{coil}}=U_{\mathrm{r2}}^{\mathrm{banding}},U_{\mathrm{r1}}^{\mathrm{coil}}=U_{\mathrm{r1}}^{\mathrm{bobbin}},\ \tau_{\mathrm{r1}}^{\mathrm{coil}}=\tau_{\mathrm{r1}}^{\mathrm{bobbin}},\tau_{\mathrm{r2}}^{\mathrm{coil}}=\tau_{\mathrm{r2}}^{\mathrm{banding}}$$

$$U_r(r,z)=\sum_{i=0}^{m}u_i^r(r)z^{2i},\quad U_z(r,z)=\sum_{i=0}^{m}u_i^z(r)z^{2i\text{-}1} \tag{12}$$

where, $u^r{}_i(r)$ and $u^z{}_i(r)$ are undetermined subfunction, and m = 4.

Replacing Eq.(12) with Eqs.(10) and (11), the partial differential equations are translated into the ordinary differential equations, and the z coefficient is zero. Therefore, there is an ODE group solved by using boundary conditions of the coil, bobbin and banding [12], where r_0 and r_1 are an inner radius of the bobbin and the coil, r_2 and r_3 are accordingly an outer radius, and p_{cover} is a radial stress of the cover plate.

3.4 Stress induced by magnetic load

In the case of electromagnetic stress, temperature difference of the coil is zero at sufficient cooling, then the partial differential equations should include the body force:

$$r^2\frac{\partial^2 U_{\mathrm{r}}}{\partial r^2}+a_{\mathrm{r1}}r^2\left(\frac{\partial^2 U_{\mathrm{z}}}{\partial r\partial z}\right)+a_{\mathrm{r2}}r^2\frac{\partial^2 U_{\mathrm{r}}}{\partial z^2}+r\frac{\partial U_{\mathrm{r}}}{\partial r}+a_{\mathrm{r3}}r\frac{\partial U_{\mathrm{z}}}{\partial z}+a_{\mathrm{r4}}U_{\mathrm{r}}+a_{\mathrm{r5}}r^2F_{\mathrm{r}}=0 \tag{13}$$

$$r\frac{\partial^2}{\partial z^2}U_z+a_{z1}r\left(\frac{\partial^2}{\partial r^2}U_z\right)+a_{z2}r\left(\frac{\partial^2}{\partial z\partial r}U_r\right)+a_{z3}\frac{\partial U_r}{\partial z}+a_{z1}\frac{\partial U_z}{\partial r}+a_{z4}rF_z=0 \tag{14}$$

where, a_{r1} to a_{r5} and a_{z1} to a_{z5} are constant in stiffness elements, and the body forces are described as a power series polynomial form:

$$F_r(r,z)=\sum_{i=0}^{m}\left(A_i^{r1}+A_i^{r2}r\right)z^{2i},$$

$$F_z(r,z)=\sum_{i=1}^{m}\left(B_i^{z1}r^2+B_i^{z2}r+B_i^{z3}\right)z^{2i\text{-}1} \tag{15}$$

where, A_i^{r1}, A_i^{r2}, B_i^{z1}, B_i^{z2}, and B_i^{z3} are determined by a given magnetic field.

Considering the z coefficients as zero, a new ODE group can be obtained by substituting Eqs.(11) and (15) with Eqs.(13) and (14). Although it includes body force, the form of boundary conditions is the same as that of thermal stresses.

Table 1 Specification of the magnet with 2.58 m bore.

Parameter	Value
Inner diameter (mm)	1350
Outer diameter (mm)	1450
Axial length (mm)	96
Thickness of banding (mm)	23
Thickness of bobbin (mm)	10
Number of layers	45
Current density in conductor (A/m^2)	2.02×10^8

The designed criterion of the coupling coil assembly is that the materials do not have a plastic deformation. The Mises yield criteria is used to examine the mechanical safety of the coil assembly:

$$\sigma_{\mathrm{VM}} = \sqrt{\frac{1}{2}\left[\left(\sigma_r-\sigma_\theta\right)^2+\left(\sigma_\theta-\sigma_z\right)^2+\left(\sigma_z-\sigma_r\right)^2+6\tau_{rz}\right]} \quad (16)$$

4 Stresses solutions

4.1 Model verification

To verify the model, the stresses is calculated by using the analytical model within a Russia superconducting magnet[13], with a room temperature bore of 2.58 m. The mandrel and banding are made of stainless steel. Main parameters of the coil are listed in Table 1. The model assumed that the coil is isotropic so as to conform with the reference. The winding tension applied on the conductor and banding are 230 and 55 MPa, respectively. From Table 2, the analytical results are close to the report described previously[13].

Table 2 Results comparison

Results		Max. radial displacement /mm	Radial pressure to bobbin /MPa	Max. hoop stress /MPa
Cooling	I*	3.600	10.200	116
	II*	3.677	11.024	122
Charging	I	-	8.700	153
	II		9.667	160

4.2 Stress in the MICE coupling coil assembly

The properties of materials of the MICE coupling coil assembly are given in Table 3. The elastic modulus in the radial, hoop and axial directions are E_r, E_θ and E_z, and the Poisson ratios are in turn $v_{r\theta}$, $v_{\theta z}$ and v_{rz} in corresponding directions. The winding tensions applied to the conductor and banding are both 60 MPa.

Figure 2 shows the distribution of radial stress in the MICE coupling coil assembly. From room temperature to 4.2 K, the radial pressure on the bobbin decreases to –3 MPa at the current of 210 A. It means that there is no gap between the coil package and the bobbin. The largest radial stress is about –27 MPa in the central layers of the coil due to the magnetic load.

Considering slip plane effect in the finite element model, the charged results are smaller than the analytical results. The slip planes release the radial and shear stress due to relative sliding of the coil to the mandrel.

Table 3 Properties of materials

Property	Bobbin	Coil Winding	Banding
E_θ/GPa	77.1	69	71
E_r /GPa		52	
E_z /GPa		94	
G_{rz}/GPa	29.2	34.62	27.31
$v_{r\theta}$	0.31	0.34	0.32
$v_{\theta z}$		0.32	
v_{rz}		0.2	
a /K^{-1}	1.42×10^{-5}	1.149×10^{-5}	1.41×10^{-5}

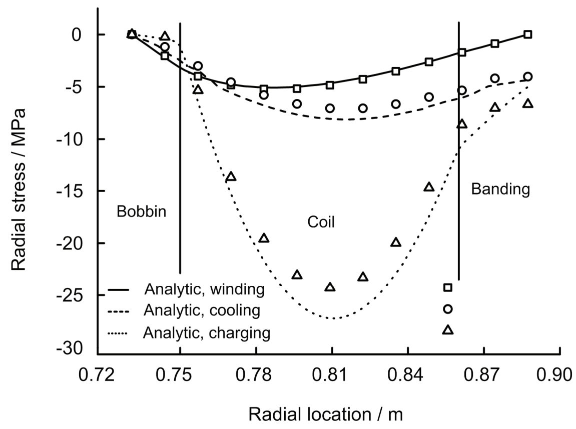

Fig.2 Radial stress in the mid-plane of the coil assembly.

The hoop force is influenced more higher than the radial force by the thermal contraction and magnetic load (Fig.3). The hoop stress in the coil increases monotonically with the radial location due to the winding tension and the maximum stress occurs when the electromagnetic force reaches the peak value, which is 150 MPa appears in the banding. Although the outward Lorentz force pushes the coil along radial direction, the inward pressure from winding tension offsets the effect of that. Furthermore, the banding restricts the movement of the coil, so the hoop stress in the inner layers is always negative.

The axial stress is nearly linear with the radial location in the midplane of the coil after cooling (Fig. 4), which reaches the maximum of –57 MPa at the current of 210 A. The calculation results of finite element model are larger than the analytical values. This indicates some degree of inward bending occurring in the coil.

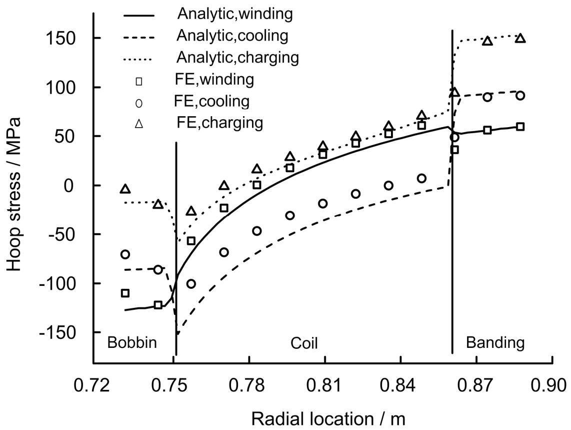

Fig.3 Hoop stress in the mid-plane of the coil assembly.

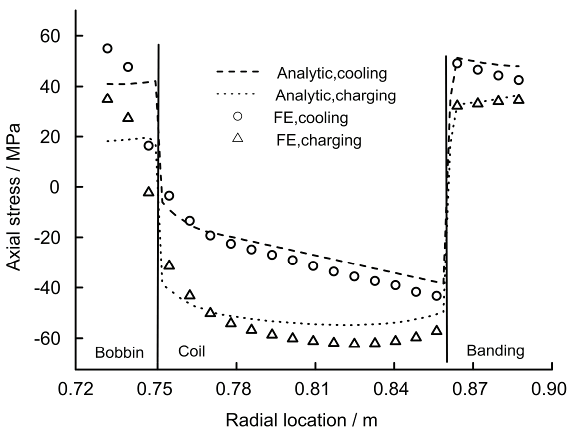

Fig.4 Axial stress in the coil assembly in mid-plane of the coil.

Not affecting the safety of the structure, the shear stress in the coil is important for the stability of the magnet. The shear stress is created by the restraint of the coil package against movement alone its boundaries, thereby it is small in the mid-plane, but is large in the ends of the coil so that one focus on the end of the coil (Fig.5). The shear stress mainly concentrates in the top and bottom corner of the coil package. In which the latter changes from 30 MPa to 18 MPa as the coil is energized because the radial Lorentz force reduces the interactions of the coil and the mandrel. The finite element solution changing more smoothly, the peak value of shear stress is smaller than that of the analytical results, which is due to that slip planes decrease the constraints of the coil package in the finite element model.

The critical point is checked by Von Mises stress distribution in the coil assembly (Table 4). The highest stresses in the mandrel and coil are respectively 138 and 127 MPa at 4.2 K, and 142 MPa in the banding caused by magnetic load. Compared with the yield limit of materials, the highest stresses in the three sections of the coil assembly are in the allowable stresses of materials at cryogenic temperature. The largest stress is lower than the allowable stress of 5356 aluminum at 4.2 K.

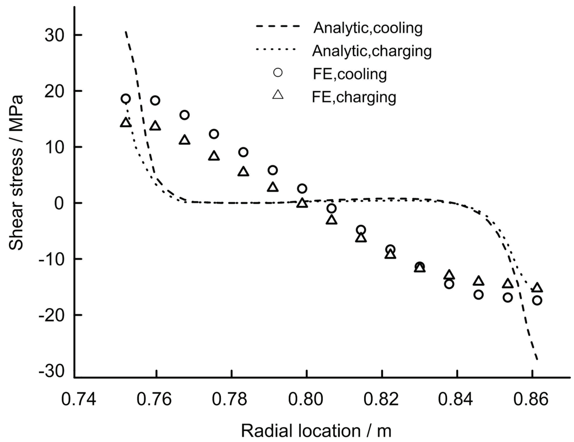

Fig.5 Shear stress in coil assembly at the end of coil package.

The analytical solutions are generally in agreement with the simulations, but the effect of the inward bending and slip planes is underestimated in the analytical model, which causes that the axial pressure in the mid-plane is smaller and the shear stress in the corners of the coil is larger by contrasting with the finite element simulation. Although the analytical model introduces some assumptions, it provides a theoretical verification for the finite element results.

5 Discussion on mechanical stability

Epoxy resin used as the impregnate material serves to keep the coil intact during cool down and energization.

However, because epoxy has low strength at cryogenic temperature and stress-induced failures, cracking in the epoxy is a general way to cause a quench or training in a thick superconducting solenoid[14]. The Lorentz force and stress concentration are the main source of epoxy cracking:

(1) In the analogous magnets with a large scale bore, the radial strain is in the range of 0.04–0.05% when training starts[13]. The maximum radial strain of the analytical solution caused by the magnetic load is 0.034%, which is less than the upper limit of 0.05%.

(2) The shear stress concentrates in the bottom corner of the coil package due to the restraints of the coil form, which appears as principle stresses. The modes of stress-induced failure of the epoxy at cryogenic temperature are tensile and shear crack. Therefore, if the magnitude of the principle stresses or the maximum shear stress is greater than the strength of epoxy (its tensile and shear strength are 30 and 17 MPa), the cracking will occur. The principle stress is defined as:

$$\sigma_p^3 - I_1\sigma_p^2 + I_2\sigma_p - I_3 = 0 \tag{17}$$

where, σ_p is a principle stress; I_1, I_2 and I_3 are the 1st, 2nd and 3rd stress invariant which is calculated by:

$$\begin{aligned} I_1 &= \sigma_r + \sigma_\theta + \sigma_z \\ I_2 &= \sigma_r\sigma_\theta + \sigma_\theta\sigma_z + \sigma_r\sigma_z - \tau_{rz}^2 \\ I_3 &= \sigma_r\sigma_\theta\sigma_z - \sigma_\theta\tau_{rz}^2 \end{aligned} \tag{18}$$

The first principle stress and the maximum shear stress in the bottom corner of the coil are about 22 MPa and 50 MPa so that the shear stress makes the epoxy resin cracked, and further causes a quenching or training by charging the magnet.

6 Conclusion

The static stress solution for the coupling coil assembly used in the MICE cooling channel is obtained by the combined cylinder theory and power series expansion. The theoretical calculation coincides well with the finite element simulations. The magnet does not undergo plastic deformation during the cool down and energization. The finite element technique is always available for the detailed analysis. The analytical technique can be used as theoretical principle for a finite element program. From the analysis, the maximum shear stress in the coil is close to the fractured toughness of epoxy, which may cause quenching or training effect due to the cracking of epoxy resin.

References

1 Wang L, Xu F Y, Wu H, *et al.* IEEE Trans. Appl Supercond, 2009, **19(3):** 1344–1347.

2 Wang L, Green M A, Xu F Y, *et al*. IEEE Trans Appl Superconduc, 2008, **18(2):** 937–940.

3 Li D R, Green M A, Virostek S P, *et al*. Proceedings of 2005 Particle Accelerator Conference, Knoxville, TN, 2005, 3417–3420.

4 Gray W H, Ballou J K, J Appl Phys, 1977, **48(7):** 3100–3109.

5 Mitchell N, Mszanowski U, IEEE Trans Magn, 1992, **28(1):** 226–229.

6 Markiewicz W D, Vaghar M R, Dixon I R, *et al*. J Appl Phys, 1999, **86(12):** 7039–7051.

7 Vaghar M R, Garmestani H. J Appl Mech, 2001, **68**: 11–18.

8 Cox W, Garmestani H, Markiewicz W D, *et al*. IEEE Trans Magn1996, **32(4):** 3012–3015.

9 Pan H, Wang L, Wu H, *et al.* Cryogen Supercond, 2009, **37(8)**: 14–17(in Chinese).

10 Wilson M N. Monographs on Cryogenics Superconducting Magnets. Oxford, Oxford University Press, 1983: 41–50.

11 Bobrov E S, Williams J E C. IEEE Trans Appl Supercond, 1981, **17(1):** 447–448.

12 WANG Q L. Science of high field superconducting magnets. Beijing, Science Press, 2008: 157–163 (in Chinese).

13 Karasik V R, Kleshnina O A, Konjukhov A A, *et al*. Proceedings of Advances in Cryogenics Engineering, New York, 1992, **37A:** 40-48.

14 Iwasa Y. IEEE Trans Magn, 1991, **28(1):** 113–120.